DAA/AMES

STRUCTURAL CHARACTERIZATION AND GAS REACTIONS OF SMALL METAL PARTICLES BY HIGH RESOLUTION IN-SITU TEM AND TED

Semi-Annual Technical Report

for the period
July 1, 1985 - September 30, 1985

Submitted to

National Aeronautics and Space Administration
Ames Research Center
Moffett Field, California 94305

Aerothermodynamics Branch
Dr. Dave Cooper, Acting Chief

NASA-Grant NCC2-283

Prepared by

ELORET INSTITUTE
1178 Maraschino Drive
Sunnyvale, CA 94087
(phone: 408 730-8422)
K. Heinemann, President and Principal Investigator
13 January, 1986

STRUCTURAL CHARACTERIZATION AND GAS REACTIONS OF SMALL METAL PARTICLES BY HIGH-RESOLUTION IN-SITU TEM AND TED

The modification of the in-situ TEM facility for improved vacuum and sample handling capabilities has been completed. A base pressure of 5×10^{-10} mbar can now be obtained in the sample chamber system, and the sample can be exchanged through an airlock arrangement within 15 minutes, while the pressure exceeds at no time 3×10^{-7} mbar. A major paper describing this work is now in print at J. Vacuum Science & Technology. A copy of this submittal is attached as Appendix A.

An extensive paper on the influence of the electron beam during high-resolution transmission electron microscopy of small supported metal particles is now in print in Ultramicroscopy. The contents of that paper is essentially congruent with our Semi-Annual Technical Report on this grant (NCC2-283) for the period 1/1/85 - 6/30/85, submitted on 7/15/85.

APPENDIX A

AN ULTRA-HIGH VACUUM MULTIPURPOSE SPECIMEN CHAMBER WITH SAMPLE INTRODUCTION SYSTEM FOR IN-SITU TEM INVESTIGATIONS

K. Heinemann
Eloret Institute, 1178 Maraschino Drive, Sunnyvale, CA 94087

and H. Poppa
Stanford/NASA Joint Institute for Surface and Microstructure Research, NASA-Ames Research Center, Moffett Field, CA 94035

ABSTRACT

A commercial electron microscope with flat-plate upper pole piece configuration of the objective lens and top entry specimen introduction was modified to obtain $5*10^{-10}$ mbar pressure at the site of the specimen while maintaining the convenience of a specimen airlock system that allows operation in the 10^{-10} mbar range within 15 minutes after specimen change. The specimen chamber contains three wire evaporation sources, a specimen heater, and facilities for oxygen or hydrogen plasma treatment to clean as-introduced specimens. Evacuation is achieved by dual differential pumping, with fine entrance and exit apertures for the electron beam. The microscope operating at 10^{-6} mbar, the first differential pumping stage features a high-speed cryopump operating at a stainless steel chamber that can be mildly baked and reaches $1*10^{-8}$ mbar. The second stage, containing the evaporation sources and a custom ionization gauge within 10 cm from the specimen, is a rigorously uncompromised all-metal uhv-system that is bakable to above 200 C throughout and is pumped with an 80-liter ion pump. Design operating pressures and image quality (resolution of metal particles smaller than 1 nm in size) were achieved.

I. INTRODUCTION

Ever since Moorhead and Poppa (1) reported in 1969 the successful construction of a uhv specimen chamber fitted to a transmission electron microscope, in-situ TEM experimentation under controlled vacuum conditions has been a desirable and powerful technique employed in many areas of thin film and surface physics research. Moorhead and Poppa essentially separated a commercial TEM between the condenser and objective lenses and inserted a custom designed, metal-sealed stainless steel chamber that contained new specimen x-y movement facilities and various peripheral equipment for in-situ experimentation, such as evaporation sources and a residual gas analyzer. The chamber was pumped separately from the microscope with two Orbion pumps; and the electron beam entered and exited via small apertures. For best vacuum conditions, a liquid helium cryopump could be activated to increase the pumping speed.

During the following 15 years, their approach has been steadily refined in this laboratory and employed in a wide variety of research activities, including in-situ epitaxial nucleation and growth measurements (2), the in-situ preparation of clean electron-transparent films such as alumina (3,4) and MgO (5) and their use as substrates for in-situ metal depositions (4,6), oxidation of copper and Cu/Ni alloys (7-9), in-situ cluster mobility studies (10-13), in-situ low-pressure chemical vapor deposition studies of silicon on sapphire (14), and in-situ reactions of metal/substrate systems of catalytic importance (15-18). The instrumental improvements included fitting this type of in-situ chamber to a higher-resolution Siemens Elmiskop 101 microscope

(7), replacing the Orbion pumps with a (mechanical) helium cryopump (19) or a Vacion pump (20), using a sputter-ion gun for in-situ cleaning of substrates (21), and instituting a jet for in-situ gas (7-9, 14, 17-19) and plasma treatment (20) at higher pressures in the vicinity of the specimen.

A fundamentally different approach for obtaining uhv conditions at the site of the specimen for performing in-situ TEM experiments has been implemented by as early as in 1965 by Poppa (22) and was later perfected by Honjo, Yagi, and coworkers (23, 24). Leaving the basic configuration of condenser lens, objective lens, and specimen table essentially unchanged, the immediate vicinity of the specimen was surrounded with cryogenic surfaces. This approach found a number of excellent high resolution in-situ TEM applications by the latter group of researchers (25,26). Many of these applications are referenced in a review paper on in-situ TEM work by Honjo and Yagi (24), who more recently extended this "cryo-cage" approach to include reflection electron microscopy (27-29). The cryo-cage method of uhv, in-situ TEM has the distinct advantage over the "uhv-chamber" approach (1) that it is easier to maintain the high-resolution capability of the original microscope, while the latter involves the construction of a new specimen table, operated with metal bellows only, a requirement which is prone to resolution- compromising complications. Another difficulty in the latter approach has been an inherent increase in the objective focal length, due to the necessity to insert a differential pumping aperture in the tight space between the specimen and the objective aperture. This disadvantage of an increased focal length, which is concomitant with increased spherical and chromatic aberrations, could

only recently be eliminated (19). An inherent disadvantage of the cryo-cage approach is that it does not lend itself to a direct measurement of the vacuum at or near the specimen with a standard ionization gauge. Poppa (22) actually described a custom miniature discharge gauge for which the necessary magnetic field was supplied by the TEM objective lens and which was used down to the mid 10^{-8} mbar range, but it is questionable if this design can be adapted to accurate measurements in the 10^{-10} mbar range and in cases where the immediate vicinity of the objective lens gap is not accessible for a cold cathode electrode. Normally, the actual pressure at the site of the specimen in the cryo-cage approach is only estimated using assumptions about sticking coefficients at the cryogenic surfaces and impingement directions under which residual gas molecules stemming from the regular TEM vacuum are intercepted by cold surfaces. Due to the various openings required in the cryogenic vessel, such as for insertion of the specimen and the objective aperture, as well as due to the proximity of the upper differential pumping aperture to the specimen, a relatively high probability exists for gaseous molecular beams to reach the specimen. Furthermore, the controlled pumping of hydrogen is generally difficult in the cryo-cage approach. Recent experience we gained with a commercial cryopump indicates that the hydrogen partial pressure increases rapidly as soon as the temperature of the cryogenic surfaces exceeds 18°K.

The trend set to some extent by these two research groups (1-22, and 23-29) has resulted in a general attempt by manufacturers of high-performance transmission electron microscopes to improve the vacuum at the site of the specimen. This has been done by employing a

second pump -- an oil diffusion pump, using a low vapor pressure fluid or an ion pump -- connected directly to the specimen chamber, by using a copper "liner" to reduce the uncontrolled outgassing of various vacuum components in the imaging portion of the microscope, and/or by instituting a "mild" bakeout of the microscope column, in addition to other obvious measures such as the use of Viton seals throughout the column. The state of the art seems at present to be the mid 10^{-7} mbar pressure range in the specimen chamber, with some noteworthy excursions into the 10^{-8} mbar range. However, any further reduction of pressure into the true ultra-high vacuum pressure range will not be possible with any or all of these refinements of "standard" microscope design techniques. Instead, it will require implementation of true uhv design practices that allow bakeout at temperatures well above 150°C, make use of uhv compatible materials throughout, and avoid in particular non-metal seals to ambient pressure.

As will become apparent in the following, the chamber pressure in the Moorhead/Poppa approach is limited to the mid 10^{-9} mbar range primarily by the gas evolution from the chamber walls, rather than by throughput from the beam entrance and exit apertures. Reducing the ultimate pressure by one order of magnitude would require a reduction of the mean specific outgassing rate of the chamber components to a level that can only be obtained by bakeout at temperatures above 150°C throughout the chamber. This would have to include specifically the center section of the chamber with the beam entrance and exit apertures, and the Viton seals connecting the chamber with the microscope. Since the microscope lenses with aperture drives and deflection system cannot nearly withstand this temperature, a

conceptually different approach had to be persued to reduce the pressure at the site of the specimen to the mid 10^{-10} mbar range. Leaving the main in-situ chamber at its "natural" pressure limit in the high 10^{-9} mbar range, we designed a second, differentially pumped "mini"-chamber situated inside the main chamber with the following basic vacuum characteristics:

(i) very small interior surface area;

(ii) truly uhv-compatible components that can be baked to temperatures above 250°C;

(iii) specimen exchange without the necessity of renewed baking, i.e., the pressure remains in the low 10^{-9} mbar range while changing the specimen.

The minichamber was, furthermore, designed to accept evaporation sources for in-situ metal depositions while the pressure at the site of the specimen remains in the 10^{-10} mbar range.

We describe in this report the pumping and design principles, special features, and the actual performance obtained with this new uhv specimen chamber for in-situ TEM experimentation. We also extend the discussion of design principles to more general conclusions pertaining to differentially pumped uhv microscope systems.

II. DESIGN FEATURES

A schematic drawing of the in-situ TEM facility with UHV mini-specimen chamber is shown in Fig.1. A Siemens Elmiskop 101 was separated between objective lens and specimen chamber, and a custom stainless steel chamber (the main chamber), differentially pumped with a closed-loop helium cryopump, was inserted as described in earlier publications (14-19). The chamber vacuum extends through a 6 mm DIA tube in the regular TEM deflection system and ends in a 1.5 mm DIA, x-y adjustable beam entrance aperture situated shortly below the final microscope condenser (C2) aperture. The beam exit aperture of the main chamber is located in the gap between the objective lens pole pieces. A minichamber is inserted into the main chamber and is pumped with an 80 l/s ion pump through piping sections of varying length and diameter, the details of which will be described in the following section. The minichamber is mounted in the specimen table which glides on the upper objective pole piece. The specimen is inserted into a fixed position at the lower end of the minichamber. Gliding x-y specimen movement, which is accomplished by movement of the entire minichamber, is accomodated through a bellows system connecting the minichamber with its pumping section. A schematic to-scale drawing of the center portion of the main chamber with minichamber is presented in Fig.2. The minichamber furthermore contains three wire-type evaporation sources (one is schematically shown in Fig.2) and a sample heater (a heated W-ring surrounding the sample holder).

The sample is introduced with a sample introduction system (shown in Fig.2 in inserted position) and consists of (i) the sample

introduction rod which can be horizontally moved in the tube, (ii) the cylinder which is hinged to the rod, (iii) the cone which is hinged to the cylinder, and (iv) the sample holder which is connected to the cone with two wires. When the specimen is inserted, these two wires are disengaged from the actual specimen holder. To further minimize transfer of vibrations from the introduction system to the sample, the cone, when seated in the conical seat in the minichamber, is disengaged from the cylinder. Cylinder and cone contain a coaxial bore for the electron beam. The cone also contains a 1.5 mm DIA beam entrance aperture. To initiate a withdrawel of the sample from the minichamber, the sample introduction rod is pulled radially outward (to the left in Fig.2); this tilts the cylinder and brings it in contact with the guide which is dimensioned such that the cylinder, while it is moved ourward, lifts the cone vertically upward. Upon upward movement of the cone, the two wires engage in the sample holder and start lifting it. When the sample holder has cleared the conical seat in the minichamber, the lower hinge of the cylinder, still on the optic axis, has reached the horizontal level of the center of the tube, at which point also the cone and the sample holder start being tilted and are eventually drawn inside the tube. Once the sample holder has cleared the front end of the tube, the entire tube can be moved radially through the main chamber and withdrawn through an airlock arrangement.

The airlock can be pumped to high vacuum (10^{-6} mbar range) and is also designed to allow sample pretreatment such as high-pressure oxygen plasma cleaning (20). At any point during sample movement through the main chamber, the sample holder can be pushed out of the tube and exposed for (ex-situ) sample (pre)treatment, such as thermal treatment

(by lowering it into an oven mounted in the main chamber) or ion bombardment.

The conical seat in the minichamber contains a simple, gravity-operated hinged metal plate seal that automatically closes when the sample holder is withdrawn. The pumping line section (3) → (2) (see Fig.1) between the bellows and the main chamber connection contains a titanium sublimation pump and is surrounded with copper tubing for water cooling. Bakeout of the minichamber and pumping lines (4) → (2) inside the main chamber is accomplished by operating the filaments for the evaporation sources and the Ti sublimation pump (below the respective metal sublimation temperatures) as well as by heating a W-filament located in the pumping segment (4) → (3). Bakeout of the external portion of the ion pump system is by heating tapes and Al-foil heat shielding. Mild bakeout of the main chamber is performed with external heating strips and with a long internal heating filament, while the microscope lens cooling is on to avoid excess heating of vital microscope parts.

The minichamber contains a jet for in-situ gas treatments, as indicated in Fig.1, and a throttle valve to avoid overloading of the ion pump while introducing gases.

All electrical feedthroughs on the minichamber are commercial uhv "mini"flange feedthroughs. In several cases, components of the minichamber are sealed to the main chamber by parallel machined surfaces bolted together, achieving low gas conductance without gaskets.

III. PUMPING AND DESIGN PRINCIPLES

The ultimate pressure, P_u in a vacuum chamber can be expressed with the well-known equation

$$P_u = Q/S_{eff} \tag{1}$$

where Q is the gas evolution and S_{eff} is the effective pumping speed at the port of the chamber. The nominal pumping speed of the pump, S_o, is related to S_{eff} by

$$S_{eff} = \left(\frac{1}{S_o} + \frac{1}{C_o}\right)^{-1} \tag{2}$$

where C_o is the conductance of the vacuum connection between pump and chamber. For a simple cylindrical geometry of this connection, with length L and diameter D, the conductance for air can be expressed (30) as

$$C_o = \left(\frac{1}{C_D} + \frac{1}{C_L}\right)^{-1} \tag{3}$$

with $$C_L = 12.1\ D^3/L \tag{4}$$

and $$C_D = 9.11\ D^2 \tag{5}$$

If D and L are expressed in cm, the conductances result in liters per second (l/s).

For more complicated pumping systems, such as for the ion-pumped

portion in Fig.1 where n sections of various pipe lengths and diameters (see also Tab.1) are in sequence, the net conductance is

$$C_0^{(T)} = \left(\sum_m \frac{1}{C_0^{(m)}} \right)^{-1} \qquad (6)$$

and the pressure in section m (whereby m=1 denotes the section closest to the pump) is

$$p_u^{(m)} = \frac{Q^{(1)}}{S_{eff}^{(1)}} + \frac{Q^{(2)}}{S_{eff}^{(2)}} + \cdots + \frac{\sum_{k=m}^{n} Q^{(k)}}{S_{eff}^{(m)}} \qquad (7)$$

In equ.(7), $Q^{(n)}$ represents the gas evolution contribution of the section n. In particular, if the pressure is measured near the pump (m=1), equ.(7) suggests a reading of

$$p_u^{(1)} = \frac{\sum_{k=1}^{n} Q^{(k)}}{S_{eff}^{(1)}} \qquad (8)$$

i.e., the pressure reading equals the total gas evolution divided by the effective pumping speed above the pump. If the pressure of the same system is measured in the segment farthest away from the pump (m=n), we expect a reading of

$$p_u^{(n)} = \sum_{k=1}^{n} \frac{Q^{(k)}}{S_{eff}^{(k)}} \qquad (9)$$

which can be substantially higher, as is the case in our in-situ TEM facility (see Fig.1 and Tab.1). If an aperture connects two high-vacuum chambers, the one with the higher pressure being at a constant pressure p_o, the final pressure p_u in the other chamber is increased to $p_u^{(a)}$ due

to the increased gas "evolution" (throughput) $Q^{(a)}$ coming through this aperture:

$$p_u^{(a)} = \frac{Q + Q^{(a)}}{S_{eff}} = p_u + \frac{Q^{(a)}}{S_{eff}} \qquad (10)$$

The throughput $Q^{(a)}$ can be espressed in terms of the conductance $C^{(a)}$ of the aperture (calculated with equ.5) and the pressure difference between the two sides of the aperture:

$$C^{(a)} = \frac{Q^{(a)}}{p_o - p_u^{(a)}} \approx \frac{Q^{(a)}}{p_o} \qquad (11)$$

Combination of equs.(10) and (11) then gives

$$\Delta p = p_u^{(a)} - p_u = \frac{p_o C^{(a)}}{S_{eff}} \qquad (12)$$

(a) Main Chamber

Assuming that the pumping speed of the cryopump is only limited by conductance, we obtain for our specific geometric configuration (L=58.25 cm, D=20.3 cm, plus an aperture of 15.2 cm DIA) an effective pumping speed of 795 l/s; and with an approximate surface area of the chamber interior of 3 m^2 and a mean outgassing rate of 2.5×10^{-10} mbar-l $s^{-1} cm^{-2}$ (see Tab.1, col.5) of the mildly baked chamber, a final pressure of 9.4×10^{-9} mbar can be expected. When considering a 1.5 mm DIA upper and 1.0 mm DIA lower aperture connecting the main chamber with the microscope condenser and objective lenses, respectively, which are assumed at p = 1×10^{-6} mbar, a pressure increase of 2.6×10^{-10} mbar and

1.2×10^{-10} mbar can be expected in the main chamber due to these apertures, raising its total pressure to 9.8×10^{-9} mbar. The ratio of pressure in the TEM and the increase in the main chamber due to conductance through the beam entrance and exit apertures is, therefore, $1 \times 10^{-6} / 3.8 \times 10^{-10} \approx 3000$.

It is of interest to note that the principal limitation of pressure in the main chamber is clearly the gas evolution from the chamber walls and not the beam entrance and/or exit differential pumping openings. Because complete, uncompromising baking is not feasible in the main chamber (because the microscope objective and condenser lenses, as well as in particular the deflection system, can not be subjected to more than 80°C), and because a number of not perfectly UHV-compatible components, such a Viton O-rings etc., have to be used in the design of the main chamber, it is obvious that further reduction of pressure at the site of the specimen into the 10^{-10} mbar range can only be achieved with a radically different approach. The improved vaccum design concept consists of a second, differentially pumped chamber located inside the main chamber.

(b) Minichamber

The minichamber is constructed in its entirety such that bakeout in principle to 400°C and in practice to 200°C throughout is possible. This allows us to assume for our calculations a mean outgassing rate of 4×10^{-12} mbar-l-s^{-1} cm^{-2} (Tab.1, case (b)). This value is based on findings by various researchers on outgassing of baked vacuum components (31-36). The inner surface area of the minichamber is approximately 500 cm^2, and the openings for the entrance and exit of the electron beam

are 1.5 and 0.6 mm DIA, respectively.

For purposes of estimating the conductance from the minichamber to the ion pump, we are differentiating three segments (see Fig.1): the segment (4) → (3) with an effective length (counting an elbow with 1.33 times its diameter as additional length) of 25 cm, a diameter of 4 cm, and a surface area of 1000 cm^2; the segment (3) → (2) with a length of 50 cm, a diameter of 6.8 cm, and a surface area of 1000 cm^2; and the segment (2) → (1) with L=80 cm, D=10 cm, and 4000 cm^2 surface area. These parameters, using 9.8×10^{-9} mbar on the high-pressure side of the beam entrance and exit apertures of the minichamber, give the results for effective pumping speeds and pressures in the various segments listed in Tab.1, lines 12b and 13b. (In cases (a) and (c) we are listing the results corresponding to outgassing rates of 2×10^{-12} mbar-l-s^{-1} cm^{-2} and 8×10^{-12} mbar-l-s^{-1} cm^{-2}, respectively). The total contribution from the apertures into the minichamber is, of course, independent of the outgassing rate and is now 1.7×10^{-10} mbar or, if measured near the ion pump, 3×10^{-11} mbar, which is an attenuation factor of $1 \times 10^{-6} / 3 \times 10^{-11} \approx 30{,}000$ between the microscope and the ion pumped system. However, whereas the contribution of the apertures was a minor factor in determining the base pressure of the main chamber, it now represents 38% of the final pressure in the minichamber, which is now in the mid 10^{-10} mbar range.

To improve the pumping speed in the minichamber system, we are employing a titanium sublimation pump with an effective pumping speed of about 800 l/s at point (2). Tab.1, lines 14-16 give the effective pumping speeds and pressures for this TiSP- augmented case. To compute S_{eff} in point (1) for this situation, we combine the 80 l/s from the ion

pump with 420 l/s stemming from the TiSF acting through a pumping line of 10 cm DIA and 60 cm length. We further assume that the two pumps will essentially generate a uniform vacuum in the entire region (3) → (1) and that this pressure eventually equals the ratio of entire gas load (28.8 mbar-l/s for open apertures) and the combined total pumping speed of 500 l/s.

If the pressure is not measured directly at one of the points of interest for which the calculation is made, but if, for example, the ion gauge is located in a separate chamber as is shown in Fig.1, it will indicate a higher pressure determined by the effective pumping speed at the location of the ion gauge and the gas evolution in that subchamber. The corrected pressure can be computed with equ.9.

(c) Direct Impingement of Gaseous Molecular Beams Through Apertures

Irrespective of the above discussion on the vacuum characteristics of the dual differentially pumped minichamber, it is necessary to address the question of direct line-of-sight impingement on the sample of residual gas molecules from the 10^{-6} mbar vacuum of the microscope through the beam entrance and exit apertures. Since the vertical extension of the aperture orifices is small, we can assume a cosine distribution for the direction under which these gas molecules leave the apertures. The fractional pressure $\Delta p/p$ due to an orifice with radius r exerted on a specimen detail at distance b from the orifice then equals the ratio of the orifice area to the surface of the sphere with diameter b, which simplifies to

$$\frac{\Delta p}{p} \approx \frac{r^2}{b^2} \qquad (13)$$

For the actual geometries used in our in-situ facility (Fig.3), the resulting fractions are 1.1×10^{-5} and 0.017 for the beam entrance and exit apertures, respectively, from microscope to main chamber. Considering 1×10^{-6} mbar as residual microscope pressure, this gives a minute pressure increase of 1×10^{-11} torr at the top side of the specimen, but it indicates an alarming pressure increase of 1.7×10^{-8} mbar at the bottom surface of the specimen. The respective fractions for the apertures between main chamber and minichamber are 5.76×10^{-4} and 0.09, but with the main chamber pressure of 9.8×10^{-9} mbar the actual influence on the specimen is only 5.7×10^{-12} mbar at the top and 8.8×10^{-10} mbar at the bottom of the sample, respectively. The critical aperture is, therefore, the lower main chamber aperture, and these considerations indicate that protection against residual gas molecules coming in direct line-of-sight from the objective lens portion of the microscope toward the specimen can only be accomplished when using specimen support films that are entirely free of holes, and when the specimen holder itself forms a low-conductance seal with the inside wall of the minichamber (see Figs.3 and 5). Then the sample film itself acts as an effective final vacuum diaphragm and shields the top of the sample film from direct molecular beam effects.

IV. RESULTS

The expected pressures listed in Tab.1, lines 13(c) and 16(c), have essentially been obtained. After a 4-hour mild bakeout of the main

chamber, its residual pressure is typically slightly below $1x10^{-8}$ mbar. After an 8-hour bakeout of the minichamber system, the base pressure measured at the location indicated in Fig.1 and using the factory-indicated emission current for the ion gauge (4 mA) is $1x10^{-9}$ mbar. When activating the Ti sublimation pump, the reading falls to $7x10^{-10}$ mbar. One TiSP flash suffices for several hours. Since the ion gauge is located in a small subchamber with 600 cm2 surface area ($4.8x10^{-9}$ mbar l/s gas evolution) and separated from the main pumping port by a 3.5 cm DIA line of 30 cm length (13 l/s effective pumping speed), it actually reads a pressure $4.8x10^{-9}/13 = 3.6x10^{-10}$ mbar higher than the residual pressure in the pump port, and the above pressure readings must be appropriately corrected to $6.4x10^{-10}$ mbar and $3.5x10^{-10}$ mbar without and with TiSP, respectively.

Measurements of the dynamic pressure ratio between the microscope column and the minichamber were accomplished by closing the main valve above the oil diffusion pump of the microscope and observing the ratio of pressure increase in the TEM column and in the ion pump system. Without the TiSP activated, an attenuation factor of 35,000 was measured. Corresponding measurements for the main chamber yielded a factor 5000. These results are slightly better than the predicted values (30,000 and 3000, respectively).

To verify the calculated pumping speeds prevailing in the minichamber system with and without activation of the TiSP, we measured the dynamic pressure ratio between the main chamber and the ion pump system over several pressure decades while the specimen was withdrawn from the minichamber and the gravity operated hinged valve was held open, leaving a channel of 2 l/s conductance between the two chambers.

A pressure increase of $\Delta p_o = 0.022\ p_{mc}$ was measured between the ion pump and the main chamber when the TiSP was not operated, p_{mc} being the main chamber pressure. When the TiSP was operated, the relation changed to $\Delta p_{sp} = 0.0020\ p_{mc}$. The former result is in perfect agreement with the predicted increase due to this added gas load, which in accordance with equs.(1 and 8) follows the equation

$$\Delta p = p_{mc} / S_{eff}^{(1)} \ (1/S_{eff}^{(4)} + 1/C_v) \qquad (14)$$

wherin $S_{eff}^{(1)}$ and $S_{eff}^{(4)}$ are the effective pumping speeds at the locations (1) and (4) indicated in Fig. 1, and C_v is the conductance of 2 l/s between the two chambers. Using $S_{eff}^{(1)} = 80$ l/s and $S_{eff}^{(4)} = 13.9$ l/s (see Tab.1, line 7), one obtains $\Delta p_o = 0.022\ p_{mc}$, as was measured. The latter result, for activated TiSP using $S_{eff}^{(1)} = 500$ l/s and $S_{eff}^{(4)} = 17.9$ l/s (Tab.1, line 14), is $\Delta p_{sp} = 0.0035\ p_{mc}$, which is higher than the measured value and therefore suggests that the actual pumping speed obtained by activation of the TiSP is even higher than the 500 l/s assumed in our estimates.

An exchange of the specimen is typically performed while the TiSP is activated. During the entire procedure, which takes about 15 minutes, the pressure -- calibrated for the pump port (point (1), Fig.1) -- remains below 2×10^{-9} mbar and falls back to the high 10^{-10} mbar range typically within 15 minutes after re-insertion of the sample holder in the minichamber.

With Fig.4 we present an example of a fine deposit of palladium on in-situ e-beam recrystallized titania, immediately following the deposition (a) and 24 hours thereafter, while the specimen was at room temperature below 1×10^{-9} mbar vacuum conditions.

V. Discussion ad Conclusions

The results indicate two fundamental design criteria for the successful reduction of the pressure at the site of the specimen in an electron microscope by differential pumping:

First, the dependence of the ultimate pressure on the outgassing rate and the effective pumping speed (equ.1) essentially demands full bakingcapability and construction with truly uhv compatible materials. Even if, for example, our present "main" chamber was redesigned to be substantially smaller, which would naturally also mean that the effective pumping speed would be somewhat smaller because of the reduced pump port sizes, a reduction of ultimate pressure to the 10^{-10} mbar range would hardly be possible if the mean outgassing rate per unit area was the same.

Second, the differential pumping apertures must be designed with utmost care. They increase the pressure by two mechanisms, (a) by conductance-limited, isotropic gas "bleeding" from the higher microscope pressure into the chamber, raising its pressure according to equ.12, and (b) by direct impingement of molecular residual gas beams from the microscope (equ. 13), reaching the site of the specimen without ever striking a chamber wall and, thus, having no chance of being affected by any vacuum improvement effort. The former mechanism imposes strict limitations on the size of these apertures and the pressure difference between microscope and chamber that can be tolerated. For example, if in our design the main chamber pressure is raised to 1×10^{-6} mbar, the pressure increase in the minichamber due to the apertures would amount to 1.7×10^{-8} mbar and, thus entirely dominate

the vacuum in the minichamber, irrespective of how well outgassed it might be. Since the aperture diameters of 1.5 mm DIA and 0.6 mm DIA for beam entrance and exit used in our design are already the practically feasible lower limit, two-stage pumping evolves in practice as a necessary design criterium.

Direct residual gas impingement imposes strict distance requirements between the differential pumping apertures and the specimen. The most severe limitation occurs at the lower chamber seal, where objective lens pole pieces and the objective aperture (which to include in the UHV portion would represent a very substantial design complexification) limit the distance to somewhat less than twice the objective focal length. Fig.5 shows the arrangement used in our design. The upper surface of the objective pole plate is in the main chamber vacuum, and the lower seal of the main chamber is accomplished through the aperture slider arranged in the pole piece gap. Although this seal is within 1 mm of the objective aperture and 4 mm from the specimen, the direct-impingement pressure influence is with 1.7×10^{-8} mbar still intolerably high, and reliable in-situ experimentation under true UHV conditions can only be performed if the specimen grids are completely covered with a hole-free support film and if the specimen holder forms a low-conductance seal with the minichamber itself, such that the molecular beam effect from below the specimen can be eliminated. We have for this reason designed the specimen holder itself so that it is positively seated in the minichamber and seals it effectively from the main chamber (see Fig.5). Accordingly, the entire minichamber is subjected to the specimen x,y- movement -- it is gliding on the objective pole plate, and the pumping line is connected to the

minichamber with a "soft" long metal bellows to allow free movement and vibration isolation from the main chamber. The accessible field of view of the specimen is limited by the 0.6 mm diameter of the lower opening of the minichamber seal. The influence of direct impingement of residual gas molecules from above to the critical top surface of the specimen is, due to sufficiently long distances between specimen and upper apertures, in our chamber design rendered insignificant (total contribution 1.6×10^{-11} mbar).

The most effective way of eliminating the molecular beam problems associated with lower main chamber aperture is, of course, by using an impenetrable thin film window as aperture diaphragm. Although this compromises the microscope resolution, it may be a viable solution for some in-situ experiments (see "membranes" in Fig.5).

The quantitative demonstration of the existence of severe pressure gradients in any vacuum system (equs.6-10) highlights the well-known but too often overlooked or underestimated fact that the location of the ionization gauge must be carefully selected. Appropriate correction factors must be applied when deducing the actual pressure at a point of interest from distant pressure readings. In our minichamber arrangement, a pressure reading near the pump (position 1, Fig.1) must be multiplied by a factor 2.1 to give the pressure in the minichamber itself. This ratio is valid when the TiSP is not activated and increases slightly when the ion pump system is better outgassed (to 2.4 for a specific outgassing rate of 2×10^{-12} mbar-l-$s^{-1}$$cm^{-2}$). The ratio increases to about 4 when the TiSP is activated.

The concept of introducing the sample with an airlock system first into the main chamber and then into the minichamber is

advantageous because it allows the minichamber to continuously remain under UHV conditions. Starting from a routinely obtained base pressure of $1x10^{-9}$ mbar in the minichamber, the pressure never increases above $3x10^{-9}$ mbar during specimen change. This is in spite of the pressure in the main chamber rising to $1x10^{-6}$ mbar when the airlock is opened. The high pressure differential of almost 3 orders of magnitude between main chamber and minichamber during specimen introduction can be maintained because during this time the beam entrance aperture into the minichamber is automatically closed (by the gravity-operated hinged valve) and thus the main source for throughput is eliminated.

The results also indicate that it is quite permissible to sometimes seal differentially pumped vacuum systems against each other with parallel metal-on-metal surfaces, without using sealing gaskets. The conductance through tiny gaps is sufficiently small that the molecular flow through some 110 cm combined length of such seals resulted in an essentially unmeasurable and negligible pressure increase in the minichamber system.

Our results indicate that it is possible, although with considerable instrumental effort, to perform high-resolution transmission electron microscopy, including in-situ preparation and treatment of the samples, under true and verifiable uhv conditions. The basis is a dual chamber, differential pumping design which should be principle adaptable to commercial transmission electron microscopes.

ACKNOWLEDGEMENTS

This work was performed at the NASA Ames Research Center under NASA Grant NCC2-283 to Eloret Institute. We also appreciate support by Alcoa Foundation for this work. We thank Dr. Miguel Avalos-Borja for his contribution during the performance of a hv/uhv model experiment in which the validity of equ. (10) for the conceptual design of our uhv specimen chamber was verified. The substrate for Fig.4 was kindly supplied to us by Dr. Tom Allen of Optical Coatings Laboratories, Santa Rosa, California.

REFERENCES:

(1) R.D. Moorhead and H. Poppa, Proceed. 27th EMSA Meeting, Claitor's Publ., Baton Rouge, La., 1969, p.116.

(2) H. Poppa, R.D. Moorhead, and K. Heinemann, J. Vac. Sci. Technol. 11, 132, 1974.

(3) K. Heinemann, R. Anton, and H. Poppa, Proceed. 39th EMSA Meeting, Claitor's Publ., Bator Rouge, La., 1981, p.158.

(4) R. Anton, H. Poppa, and K. Heinemann, Proceed. 39th EMSA Meeting, Claitor's Publ., Baton Rouge, La., 1981, p.218.

(5) H. Poppa, R.D. Moorhead, and K. Heinemann, Nuclear Instr. and Methods 102, 521, 1972.

(6) K. Heinemann, H.K. Kim, and H. Poppa, J. Vac. Sci. Technol. 16, 622, 1979.

(7) K. Heinemann, D.B. Rao, and D.L. Douglass, Oxidation of Metals 9, 379, 1975.

(8) K. Heinemann, D.B. Rao, and D.L. Douglass, Oxidation of Metals 10, 227, 1976.

(9) K. Heinemann, D.B. Rao, and D.L. Douglass, Proceed. 33rd EMSA Meeting, Claitor's Publ., Baton Rouge, La., 1975, p.46.

(10) K. Heinemann, J.J. Metois, and H. Poppa, Proceed. 34th EMSA Meeting, Claitor's Publ., Baton Rouge, La., 1976, p.434.

(11) J.J. Metois, K. Heinemann, and H. Poppa, Appl. Phys. Lett. 29, 134, 1976.

(12) J.J. Metois, K. Heinemann, and H. Poppa, Phil. Mag. 35, 1413, 1977.

(13) J.J. Metois, K. Heinemann, and H. Poppa, Thin Solid Films 41, 197, 1977.

(14) K. Heinemann and T. Osaka, J. Crystal Growth 59, 485, 1982.

(15) H. Poppa and K. Heinemann, Optik 56, 183, 1980.

(16) R.D. Moorhead, H. Poppa, and K. Heinemann, J. Vac. Sci. Technol. 17, 248, 1980.

(17) K. Heinemann, T. Osaka, and H. Poppa, Ultramicroscopy 12, 9, 1983.

(18) K. Heinemann, T. Osaka, H. Poppa, and M. Avalos-Borja, J. Catalysis 83, 61, 1983.

(19) K. Heinemann and H. Poppa, Proceed. 10th Int. Congr. EM, Hamburg 1982, Vol.2, p.497.

(20) H. Poppa, R.D. Moorhead, and K. Heinemann, in print.

(21) K. Heinemann and H. Poppa, J. Vac. Sci. Technol. 10, 22, 1973.

(22) H. Poppa, J. Vac. Sci. Technol. 2, 42, 1965.

(23) K. Takayanagi, K. Yagi, K. Kobayashi, and G. Honjo, J. Phys. E: Sci. Instr. 11, 441, 1978.

(24) G. Honjo and K. Yagi, Current Topics in Mat. Sci., Vol. 6, E. Kaldis, ed., North Holland Publ. Co., 1980, p.197

(25) Y. Tanishiro, H. Kanamori K. Takayanagi, K. Yagi, and G. Honjo, Surf. Sci. 111, 395, 1981

(26) K. Takayanagi, Surf. Sci. 104, 527, 1981.

(27) K. Yagi, Proceed. 38th EMSA Meeting, Claitor's Publ., Baton Rouge, La., 1980, p.290.

(28) N. Osakabe, Y. Tanishiro, K. Yagi, and G. Honjo, Surf. Sci. 102, 424, 1981.

(29) N. Osakabe, K. Yagi, and G. Honjo, Jap. J. Appl. Phys. 19, L309, 1980.

(30) S. Dushman, Scientific Foundations of Vacuum Technique.

2nd. ed., J.M. Lafferty, Ed., Wiley, New York 1962, p.91.

(31) J.F. O'Hanlon, in A User's Guide to Vacuum Technology, John Whiley & Sons Publ. Co., New York, 1980, p. 140.

(32) Y.E. Strausser, Proceed. 4th Int. Vac. Congr. (1968), Inst. Phys. & Phys. Soc., London, 1969, p.469.

(33) J.R. Young, J. Vac. Sci. Technol. 6, 398, 1969.

(34) R.L. Samuel, Vacuum 20, 195, 1970.

(35) R. Dobrozemsky and G. Morew, Electron. Fis. Ap. 17, 235, 1974.

(36) R. Calder and G. Lewin, Brit. J. Appl. Phys., 18, 1459, 1967.

FIGURE CAPTIONS

Fig.1. Schematic cross-sectional drawing of TEM with differentially pumped very high-vacuum main chamber and uhv minichamber; sample introduction system not shown.

Fig.2. Schematic to-scale drawing of minichamber in main chamber with sample introduction system consisting of rod (Viton-sealed in tube), cylinder, cone with sample holder, and guide structures.

Fig.3. Geometries of e-beam entrance and exit apertures at main and minichambers.

Fig.4. Pd on in-situ e-beam recrystallized titania support, immediately following deposition (left) and 24 hours later after continuous storage in residual vacuum below 1×10^{-9} mbar (right).

Fig.5. Schematic to-scale drawing of lower portions of minichamber with sample holder, lower main chamber seal with slider, and objective aperture slider.

		Mini Chamber	(4) ↓ (3)	(3) ↓ (2)	(2) ↓ (1)	Main Chamber	Equ.	Dimension
1	diameter (D)	n/a	4	6.8	10	n/a	-	cm
2	effective length (L)	n/a	25	50	80	n/a	-	cm
3	L/D	n/a	6.3	7.4	8.0	n/a	-	-
4	approx. surface area	0.05	0.1	0.1	0.4	3.0	-	m^2
5	top entrance aperture	1.5	-	-	-	1.5	-	mm DIA
6	beam exit aperture	0.6	-	-	-	1.0	-	mm DIA
7	eff. pumping speed at (S_{eff}:)	(4) 13.9	(3) 28.8	(2) 50.3	(1) 80	795	3-6	l/s
8	pressure increase due to apertures	1.7	0.8	0.45	0.3	3.8	5,12	$\times 10^{-10}$ mba
9	specific outgassing rate, case: (a)	2	2	2	2	250	-	$\times 10^{-12}$
	(b)	4	4	4	4	250	-	mbar,
	(c)	8	8	8	8	250	-	$l\ s^{-1}\ cm^{-2}$
10	gas evolution from walls for case: (a)	1	2	2	8	7500	-	$\times 10^{-9}$
	(b)	2	4	4	16	7500	-	mbar
	(c)	4	8	8	32	7500	-	l/s
11	gas evolution thru apertures upper	2.0	-	-	-	200	-	$\times 10^{-9}$
	lower	0.3	-	-	-	100	-	mbar l/s
12	base pressure (ap. closed) for case: (a)	2.8	2.4	2.0	1.6			
	(b)	5.6	4.9	4.0	3.3	94	1,7	$\times 10^{-10}$
	(c)	11.3	9.8	8.0	6.5			mbar
13	base pressure (ap. open) for case: (a)	4.5	3.2	2.5	1.9			
	(b)	7.3	5.7	4.5	3.5	98	1,7,10	$\times 10^{-10}$
	(c)	12.9	10.6	8.4	6.5			mbar
14	ON S_{eff} at point	(4) 17.9	(3) 60	(2) 800	(1) 500		3-6	l/s
15	T/SP base press. (ap.closed) for case: (a)	0.9	0.5	0.3				
	(b)	1.8	1.1	0.5			1,7	$\times 10^{-10}$
	(c)	3.7	2.1	1.0				mbar
16	WITH base press. (ap. open) for case: (a)	2.2	0.9	0.3				
	(b)	3.1	1.4	0.6			1,7	$\times 10^{-10}$
	(c)	5.0	2.5	1.1				mbar

TAB 1 Dimensions and Results

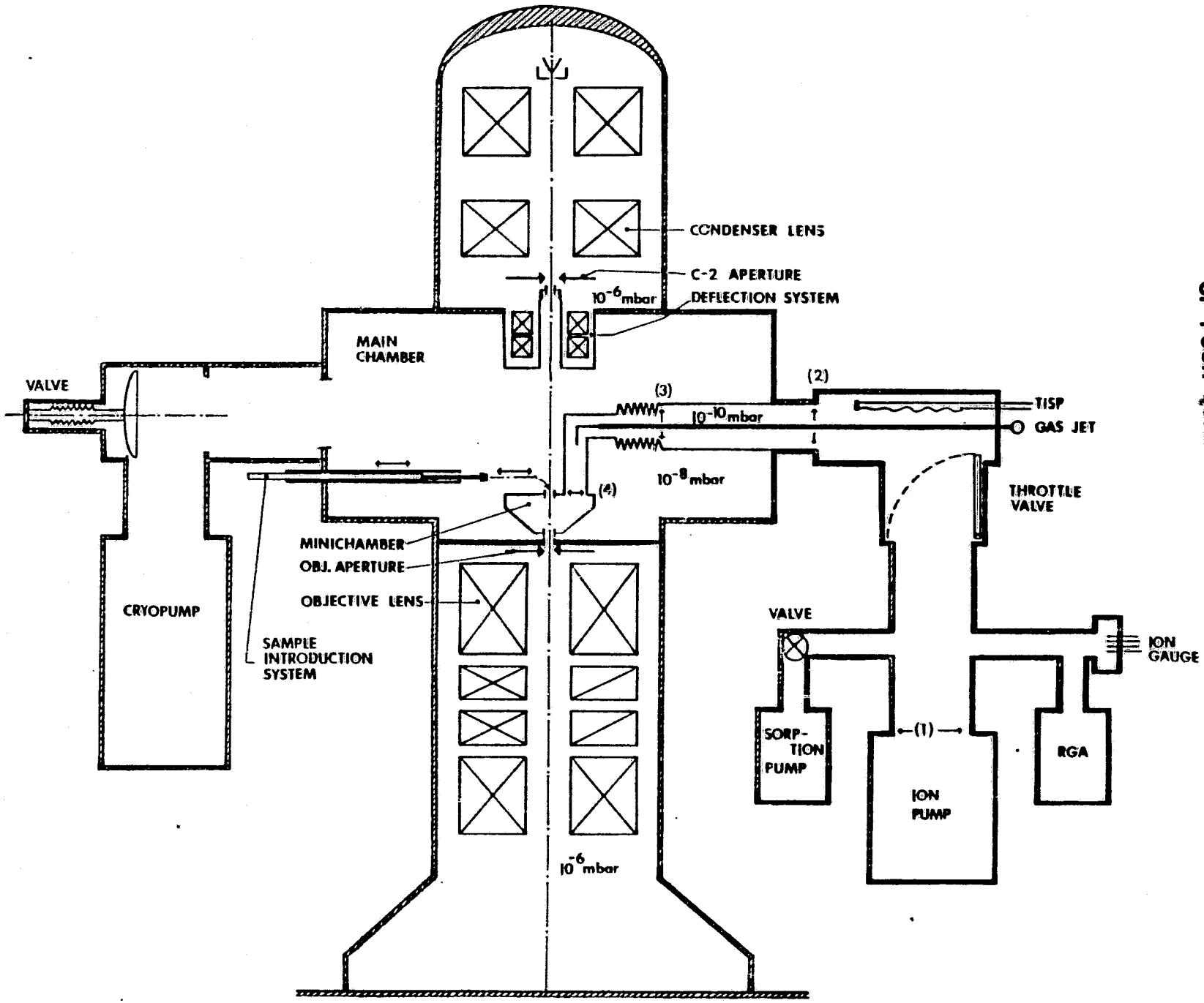

ORIGINAL PAGE IS
OF POOR QUALITY

Fig. 1

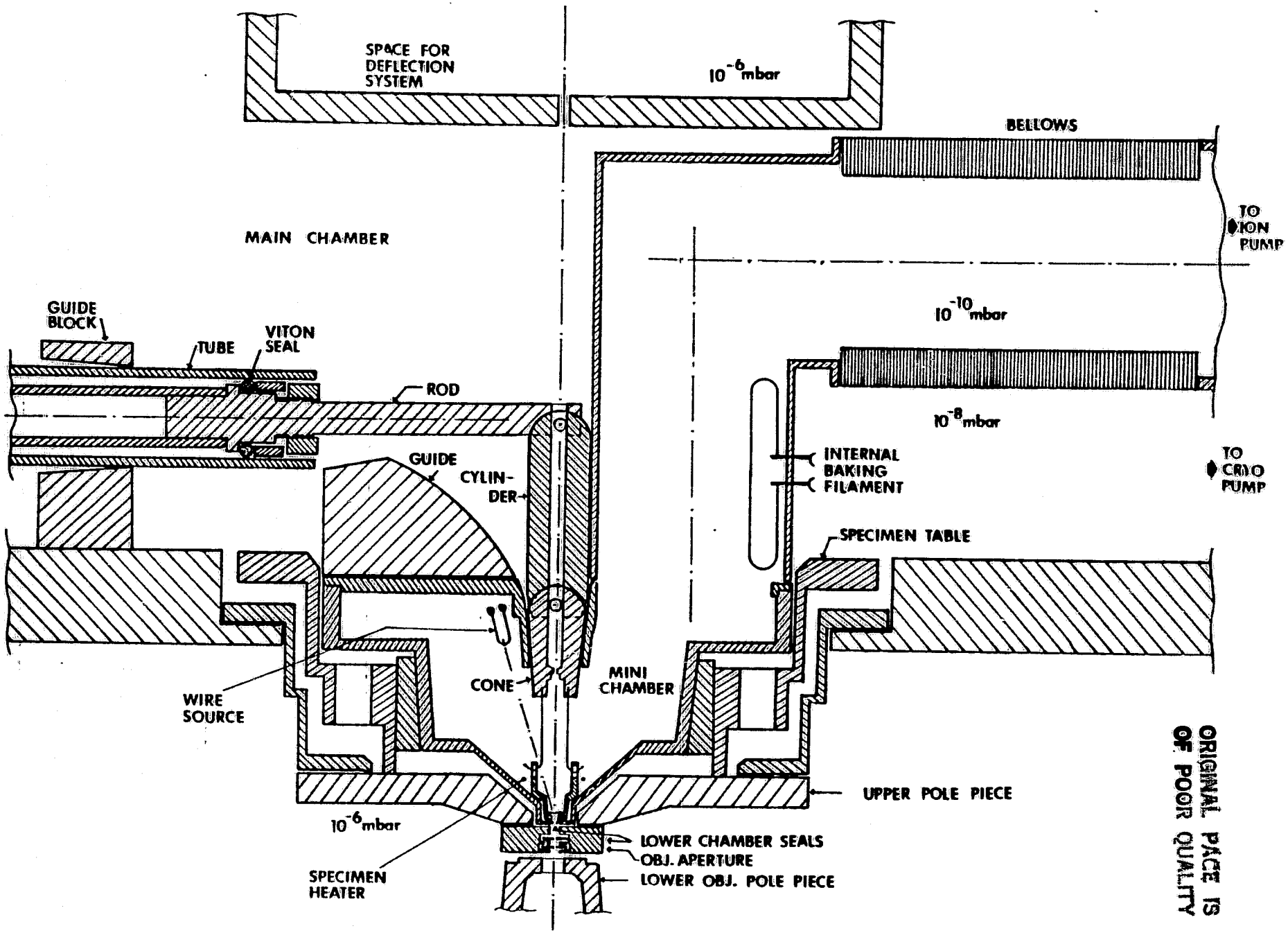

Fig-2

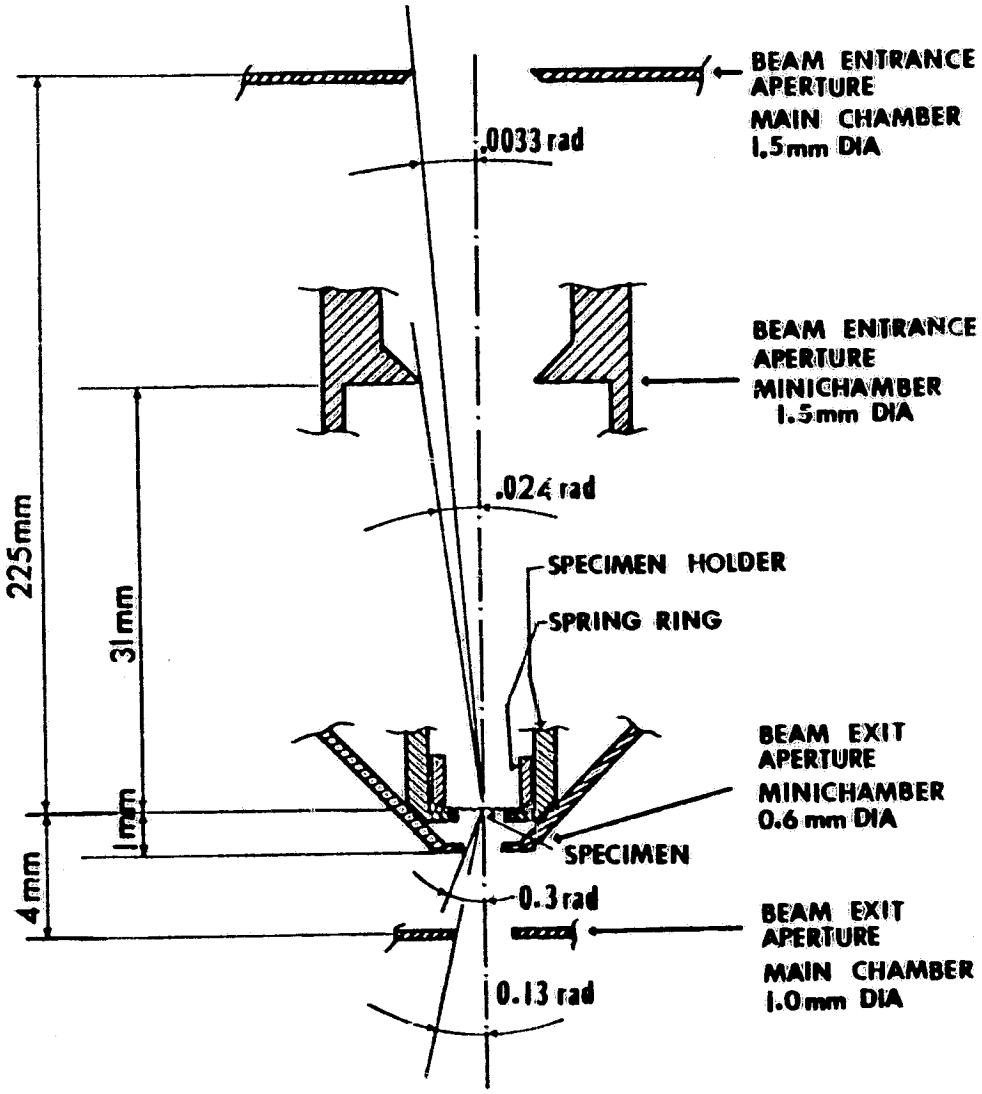
BEAM ENTRANCE APERTURE
MAIN CHAMBER
1.5mm DIA
.0033 rad
BEAM ENTRANCE APERTURE
MINICHAMBER
1.5mm DIA
.024 rad
225mm
31mm
SPECIMEN HOLDER
SPRING RING
BEAM EXIT APERTURE
MINICHAMBER
0.6 mm DIA
1mm
SPECIMEN
4mm
0.3 rad
BEAM EXIT APERTURE
MAIN CHAMBER
1.0mm DIA
0.13 rad

Fig-3

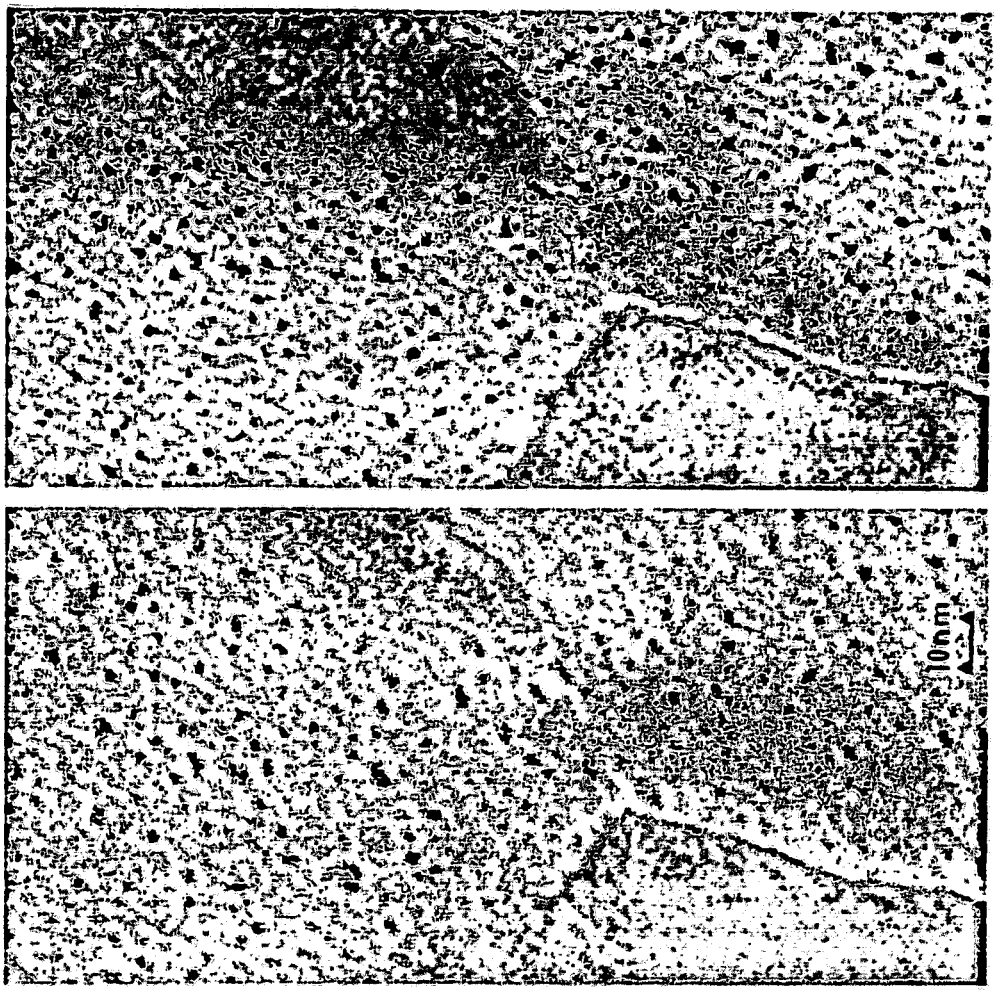

Fig.4

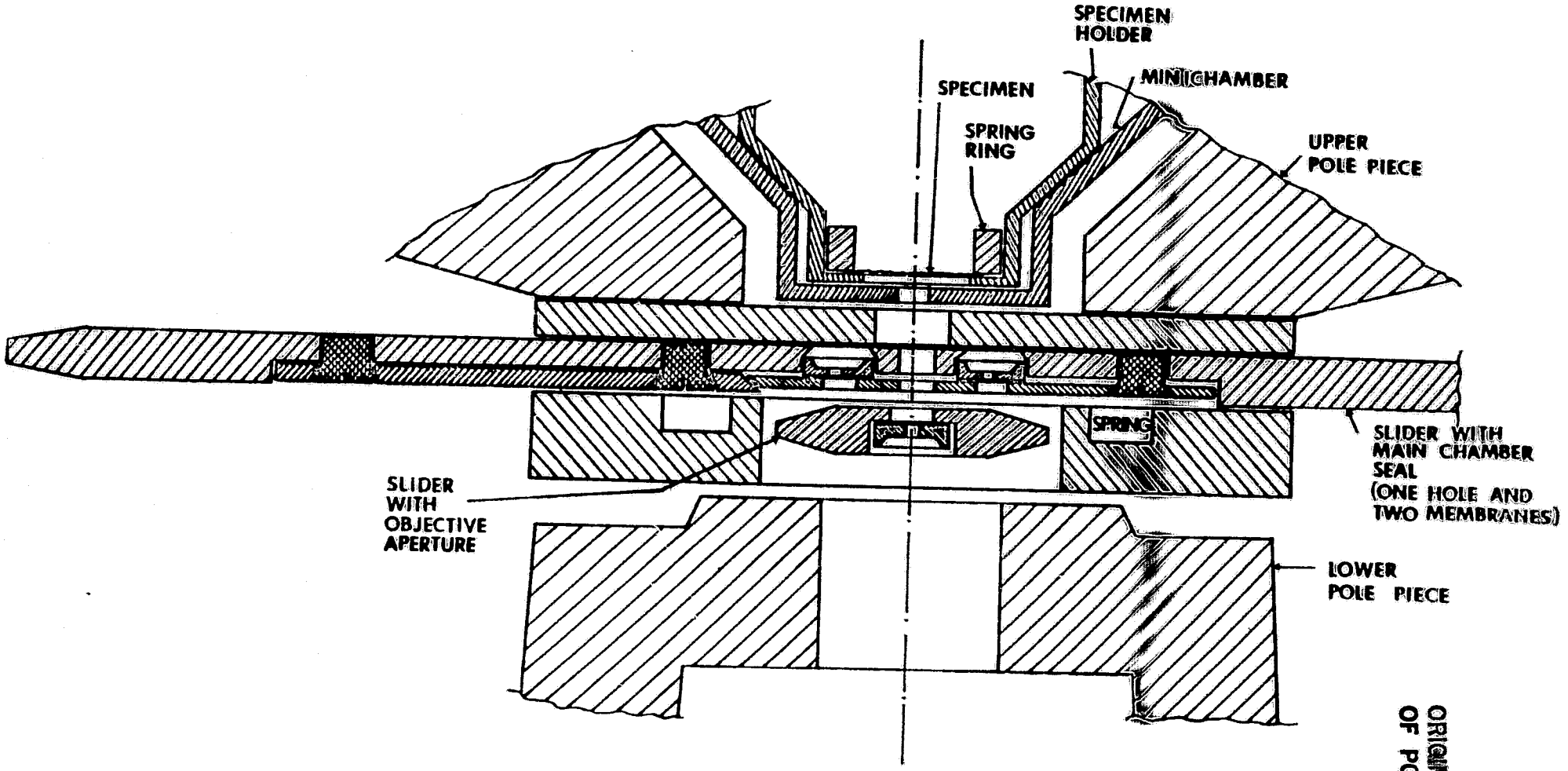

Fig. 5